Available online at www.sciencedirect.com
SCIENCE DIRECT®
International Journal of Heat and Mass Transfer 47 (2004) 4895–4910
International Journal of HEAT and MASS TRANSFER
www.elsevier.com/locate/ijhmt

Prediction of dryout and post-dryout heat transfer at high pressures using a one-dimensional three-fluid model

Sreenivas Jayanti [1], Michel Valette *

CEA-Grenoble DER/SSTH, 17 rue des Martyrs, 38054 Grenoble Cedex 9, France

Received 9 October 2003

Abstract

A set of closure relations, in the context of a one-dimensional three-fluid model, is presented for the prediction of dryout and post-dryout heat transfer at high pressure ($P/P_{cr} > 0.3$) conditions. It is shown that the traditional models based on low pressure data for interfacial friction, droplet size and the transition criteria for onset of annular flow cannot be readily extended to high pressure situations. The proposed new relations are validated by comparing with literature data in the pressure range of 30–200 bar, mass flux range of 500–3000 kg m^{-2} s^{-1} and tube inner diameters in the range of 10–25 mm. Good agreement is obtained for the dry out quality and the tube wall temperature in the post-dry out region except for cases of low mass flux at high pressures. The predictions show that at high pressure, high mass flux conditions, annular flow may prevail for low gas phase volume fraction, the droplet and the liquid film volume fractions being an order of magnitude higher than those encountered in typical air–water experiments.

1. Introduction

Dryout is an important limiting phenomenon in the design of heat exchangers and is associated with the disappearance of the liquid film on the wall in a heat exchanger tube. A consequence of this non-wetting of the heated surface is the deterioration of the convective heat transfer mechanism resulting in a large rise in the wall temperature in a heat flux imposed system such as a nuclear reactor. Since dryout is a hydrodynamic phenomenon involving entrainment and redeposition of droplets as well as boiling/evaporation of the liquid, the location of dryout is dynamic and its fluctuation may also give rise to thermal fatigue, corrosion and other problems. A large number of experimental and theoretical studies have been conducted over the past several decades to understand and quantify the processes leading to dryout in a heat exchanger tube. While empirical correlations for dryout were developed in the early stages, detailed measurements of entrainment and deposition enabled the development of "phenomenological" models for the underlying processes [1,2] and eventually to prediction of dryout based on mass balance equations [3]. Later studies extended this to include thermal non-equilibrium conditions and to a wider range of flow conditions including transient flow situations [4]. While some issues remained unresolved (such as the onset of annular flow and the entrainment fraction at the start of annular flow), this approach gave good predictions of dryout for a range of flow situations for tubes, annuli and rod bundles for pressures up to 70 bar for a steam–water system.

A more recent trend in the prediction methodology is the incorporation of these phenomenological models in a three-fluid model framework in which the full set of conservation equations (mass, momentum and energy conservation equations) are solved for three phases, namely, the liquid film, the liquid droplets and the vapour. These are incorporated in computer codes such as FIDAS [5], MONA [6], COBRA-TF [7], NEPTUNE [8]. In these codes, one-dimensional phase-averaged, time-dependent equations are solved which enable the

* Corresponding author.
E-mail addresses: sjayanti@iitm.ac.in (S. Jayanti), michel.valette@cea.fr (M. Valette).
[1] On leave from IIT-Madras, India.

0017-9310/$ - see front matter © 2004 Elsevier Ltd. All rights reserved.
doi:10.1016/j.ijheatmasstransfer.2004.03.028

Nomenclature

A	flow cross section area (m^2)
C_d	drag coefficient of droplets in gas
C_l	friction coefficient of continuous liquid on pipe wall
C_v	friction coefficient of gas on pipe wall
D_h	pipe hydraulic diameter (m)
f_i	interfacial friction factor
g	acceleration due to gravity ($m\,s^{-2}$)
H	specific enthalpy ($J\,kg^{-1}$)
k_d	deposition velocity due to diffusion ($m\,s^{-1}$)
k_q	inhibition deposition velocity ($m\,s^{-1}$)
k_s	equivalent sand grain roughness height (m)
$k_1(\alpha)$	multiplicative function for vanishing phase behaviour
Ku_v	Kutadelatze dimensionless number: $Ku_v = \alpha_v V_v \left(\frac{\rho_v^2}{[g\sigma(\rho_l - \rho_v)]} \right)^{\frac{1}{4}}$
$\dot{m}_{lfc}$	critical liquid film mass velocity ($kg\,m^{-2}\,s^{-1}$)
Nu	Nusselt number
P	static pressure (Pa)
p_{ilcv}	pressure at the interface between continuous liquid and gas (Pa)
p_{ildv}	pressure at the interface between dispersed liquid and gas (Pa)
Pr	Prandtl number $= \mu C_p/\lambda$
q	heat flux ($W\,m^{-2}$)
q_{lci}	heat flux between continuous liquid and its interface with gas ($W\,m^{-3}$)
q_{ldi}	heat transfer per unit volume between dispersed liquid and its interface with gas ($W\,m^{-3}$)
q_{vic}	heat transfer per unit volume between gas and its interface with continuous liquid ($W\,m^{-3}$)
q_{vid}	heat transfer per unit volume between gas and its interface with dispersed liquid ($W\,m^{-3}$)
q_{wlc}	heat flux between wall and continuous liquid ($W\,m^{-2}$)
q_{wld}	heat flux between wall and dispersed liquid ($W\,m^{-2}$)
q_{wv}	heat flux between wall and gas ($W\,m^{-2}$)
q_{wic}	heat flux between wall and the interface gas/continuous liquid ($W\,m^{-2}$) due to direct boiling
q_{wid}	heat flux between wall and the interface gas/dispersed liquid ($W\,m^{-2}$) due to direct boiling
R	stratification ratio
Re	Reynolds number
t	time (s)
T	temperature (C)
V	phase-averaged velocity ($m\,s^{-1}$)
W_{icv}	interface velocity between continuous liquid and gas ($m\,s^{-1}$)
W_{idv}	interface velocity between dispersed liquid and gas ($m\,s^{-1}$)
X	steam quality
z	axial coordinate (m)

Greek symbols

α	volume fraction of phase
$\alpha_{k\,min}$	residual volume fraction of phase k
β	added mass coefficient
Γ	mass transfer rate between two phases ($kg\,m^{-3}\,s^{-1}$)
Γ_e	droplet entrainment rate ($kg\,m^{-3}\,s^{-1}$)
Γ_d	droplet deposition rate ($kg\,m^{-3}\,s^{-1}$)
δ	droplet diameter (m)
λ	thermal conductivity ($W\,m^{-1}\,K^{-1}$)
μ	dynamic viscosity ($kg\,m^{-1}\,s^{-1}$)
v	kinematic viscosity ($m^2\,s^{-1}$)
ρ	density ($kg\,m^{-3}$)
σ	surface tension ($N\,m^{-1}$)
τ	shear stress (Pa)
τ_{icv}	interfacial shear force per unit volume between continuous liquid and gas ($N\,m^{-3}$)
τ_{idv}	interfacial shear force per unit volume between dispersed liquid and gas ($N\,m^{-3}$)
χ_f	wetted perimeter (m)
χ_c	heated perimeter (m)

Subscripts

b	related to boiling
cond	related to conduction
conv	related to convection
cr	relating to critical point
evap	related to evaporation
d	related to deposition of droplets
e	related to entrainment of droplets
i	related to interface
k	related to phase k
lc	related to continuous liquid
ld	related to dispersed liquid
v	related to vapour or gas
w	related to wall

simulation of important thermal hydraulic phenomena such as transient rewetting. The development of the physical models, such as those for the rate of hydrodynamic entrainment, entrainment due to nucleate boiling, rate of deposition, drop size, flow regime transitions, is still in a stage of evolution [6,9–14]. In most

cases, the code development is followed by validation of the overall set of models against experimental data. Sugawara [5,9] used the data of UKAEA [15,16], RISO [17] and other sources to provide extensive validation of dryout prediction up to 70 bar for a steam–water system. Hoyer [6], who used a different set of physical laws, used the data of Becker et al. [18,19] to validate his model up to 70 bar with uniform and non-uniform axial heat flux distribution. A limited number of calculations of data at 100 bar for a mass flux of 1000 $kg\,m^{-2}\,s^{-1}$ were also reported by him. He also compared the wall temperature variation in the post-dryout region for a selected number of cases and reported good agreement. In addition to these studies, multi-dimensional calculations of annular flow, in which the governing equations in two- or three-dimensions are solved [20,21] have also been reported but have undergone limited validation.

Thus, while a lot of progress has been made in the prediction of dryout and post-dryout behaviour, the studies have been limited to about 70 bar for a steam–water system. The prediction of post-dryout behaviour has not been systematically addressed. For example, the mass flux has a significant effect on the evolution of the wall temperature in post-dryout heat transfer. This is illustrated in Fig. 1 where the inside wall temperatures measured by Bennett et al. [15] are plotted for three different flow rates. The system pressure and the inlet subcooling are nearly the same while the heat flux varies such that dryout occurs at nearly the same location. It can be seen that the temperature rise immediately after dryout is nearly the same in all the three cases; however, the subsequent variation is a strong function of the mass flux. At low mass fluxes, the wall temperature continues to rise while at high mass fluxes, it decreases monotonically. The post-dryout wall temperature variation is also strongly influenced by the heat flux and the effect is dependent on the mass flux. This is illustrated in Fig. 2 where typical wall temperature variations, taken again from Bennett et al. [15], are shown for a low mass flux case and a high mass flux case. In both cases, increasing heat flux advances the location of dryout and the temperature jump following dryout is also increased. While temperature continues to increase in the first case, in the second case, the wall temperature continues to decrease. The effect of system pressure on the post-dryout heat transfer is considerable. This is illustrated in Fig. 3 where data of Becker et al. [18] are plotted for the same inlet subcooling and mass flux but at different pressures in the range of 30–200 bar. The heat fluxes are different but are such that dryout occurs at nearly the same axial position in the tube. It can be seen that at low pressures, the wall temperature rise following dryout is very large while at high pressures, it is relatively small. It will be shown later that the entrained droplets contribute significantly to the post-dryout heat transfer and that correct modelling of this is necessary for an accurate prediction of the heat transfer.

System pressure is therefore an important factor in determining the post-dryout heat transfer

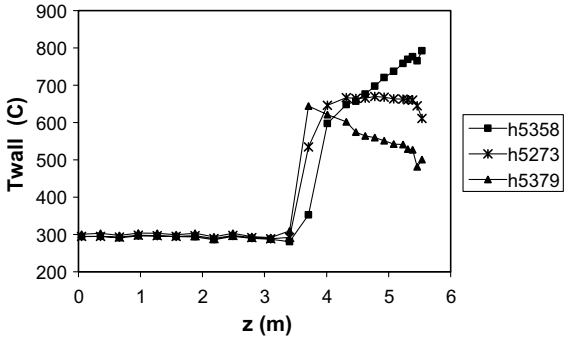

Fig. 1. Effect of mass flux on the axial variation of the inside wall temperature in the post-dryout: steam–water data of Bennett et al. [31] at 70 bar for mass fluxes of 380 (square), 1020 (asterisk) and 3800 (triangle) $kg\,m^{-2}\,s^{-1}$. The corresponding case (run) numbers are indicated in the legend.

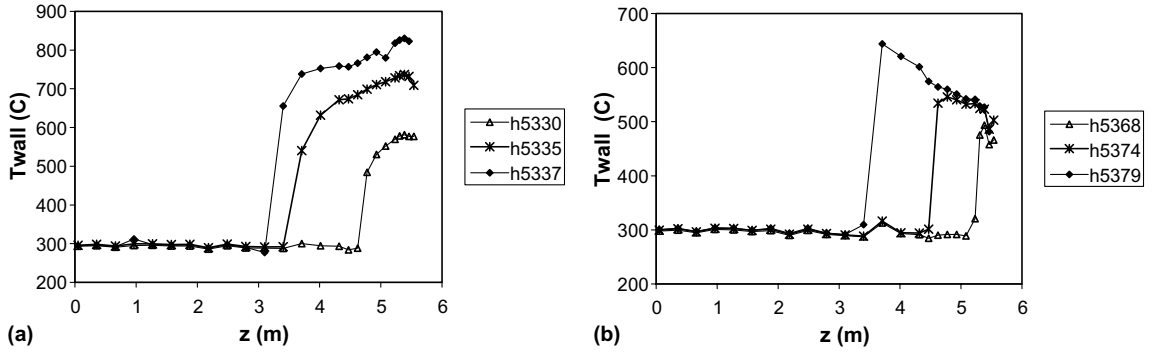

Fig. 2. Effect of heat flux on the axial variation of the inside wall temperature for (a) a low mass flux of 650 $kg\,m^{-2}\,s^{-1}$ at a heat flux of 608 (triangle), 750 (asterisk) and 848 (diamond) $kW\,m^{-2}$ and for (b) a high mass flux of 3850 $kg\,m^{-2}\,s^{-1}$ at a heat flux of 1298 (triangle), 1462 (asterisk) and 1704 (diamond) $kW\,m^{-2}$. The corresponding case numbers are given in the legend.

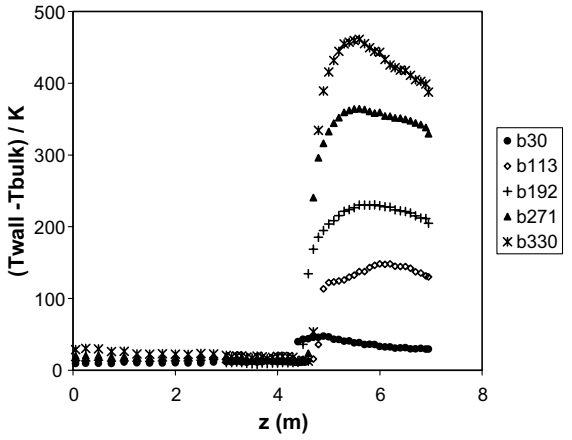

Fig. 3. Effect of pressure on the axial variation of the inside wall temperature rise in the post-dryout region: data of Becker et al. [18] at a mass flux of 1000 $\mathrm{kg\,m^{-2}\,s^{-1}}$ at a system pressure of 30 (asterisk), 70 (filled triangle), 120 (plus), 160 (diamond) and 200 (filled circle) bar. The corresponding heat fluxes are 865, 765, 458, 356 and 300 $\mathrm{kW\,m^{-2}}$, respectively. The case numbers are given in the legend.

characteristics. High pressures reduce the dryout quality and this also brings into question the transition to annular flow. The mass flux also has an effect on the dryout quality and the predictions are sensitive to the initial entrainment fraction in some cases [4]. Finally, empirical correlations for flow regime transition, interfacial friction, drop size and entrainment rate, etc. are usually based on low pressure data and may not be applicable to very high pressures. These issues are addressed in the present study in the context of a one-dimensional three-fluid formulation. The details of the framework of the calculation are presented in Section 2 while the necessary closure relations are addressed in Section 3. Numerical details of the solution scheme are briefly reviewed in Section 4. The results obtained for dryout and post-dryout heat transfer in the pressure range of 30–200 bar are discussed in Section 5.

2. Outline of the one-dimensional three-fluid model

The present three-fluid calculation scheme is based on an extension of the two-fluid model of the CATHARE code [22] and is part of the CEA-EDF NEPTUNE code project. Three sets of one-dimensional mass, momentum and energy conservation equations are solved for the three fluids, namely, gas or vapour (v), continuous liquid flowing in the form of a film (lc) and dispersed liquid flowing in the form of entrained droplets (ld). This allows for different liquid velocities and temperatures for the two liquid fields. No restrictive hypothesis has been made about the droplet temperature, which is obtained from its own energy balance equation. Thus, the model features nine independent balance equations. The corresponding main variables are the three phasic velocities V_v, V_{lc}, V_{ld}, the three phasic enthalpies H_g, H_{lc}, H_{ld}, one common pressure P and two volume fractions α_v, α_{ld} for gas and liquid droplets.

Using the notation given in the nomenclature section, the mass balance equations for the three fields can be written as follows:

Continuous liquid field

$$\frac{\partial}{\partial t}(A\alpha_{lc}\rho_{lc})+\frac{\partial}{\partial z}(A\alpha_{lc}\rho_{lc}V_{lc})=+A(\Gamma_d-\Gamma_e-\Gamma_{lcv}) \tag{1}$$

Dispersed liquid field

$$\frac{\partial}{\partial t}(A\alpha_{ld}\rho_{ld})+\frac{\partial}{\partial z}(A\alpha_{ld}\rho_{ld}V_{ld})=-A(\Gamma_d-\Gamma_e+\Gamma_{ldv}) \tag{2}$$

Gas field

$$\frac{\partial}{\partial t}(A\alpha_{v}\rho_{v})+\frac{\partial}{\partial z}(A\alpha_{v}\rho_{v}V_{v})=+A(\Gamma_{lcv}+\Gamma_{ldv}) \tag{3}$$

The momentum balance equations are written as:

Gas phase

$$\begin{aligned}&A\alpha_v\rho_v\left[\frac{\partial V_v}{\partial t}+V_v\frac{\partial V_v}{\partial z}\right]+A\alpha_v\frac{\partial P}{\partial z}-Ap_{ilcv}\frac{\partial\alpha_{lc}}{\partial z}-Ap_{ildv}\frac{\partial\alpha_{ld}}{\partial z}\\&+A\beta\alpha_v\alpha_{lc}\rho_m\left[\frac{\partial V_v}{\partial t}-\frac{\partial V_{lc}}{\partial t}+V_v\frac{\partial V_v}{\partial z}-V_{lc}\frac{\partial V_{lc}}{\partial z}\right]\\&=A\Gamma_{lcv}(W_{icv}-V_v)+A\Gamma_{ldv}(W_{idv}-V_v)-A(\tau_{icv}+\tau_{idv})\\&-\chi_f C_v\frac{\rho_v}{2}V_v|V_v|+A\alpha_v\rho_v g_z+\frac{R\alpha_{lc}}{4}p_{ilcv}\frac{\partial A}{\partial z}\end{aligned} \tag{4}$$

with $\rho_m=\alpha_v\rho_v+\alpha_{lc}\rho_{lc}$

Continuous liquid field

$$\begin{aligned}&A\alpha_{lc}\rho_{lc}\left[\frac{\partial V_{lc}}{\partial t}+V_{lc}\frac{\partial V_{lc}}{\partial z}\right]+A\alpha_{lc}\frac{\partial P}{\partial z}+Ap_{ilcv}\frac{\partial\alpha_{lc}}{\partial z}\\&-A\beta\alpha_v\alpha_{lc}\rho_m\left[\frac{\partial V_v}{\partial t}-\frac{\partial V_{lc}}{\partial t}+V_v\frac{\partial V_v}{\partial z}-V_{lc}\frac{\partial V_{lc}}{\partial z}\right]\\&=-A\Gamma_{lcv}(W_{icv}-V_{lc})+A\Gamma_d(V_{ld}-V_{lc})+A\tau_{icv}\\&-\chi_f C_l\frac{\rho_{lc}}{2}V_{lc}|V_{lc}|+A\alpha_{lc}\rho_{lc}g_z-R\frac{\alpha_g}{4}p_{ilcv}\frac{\partial A}{\partial z}\end{aligned} \tag{5}$$

Dispersed liquid field

$$\begin{aligned}&A\alpha_{ld}\rho_{ld}\left[\frac{\partial V_{ld}}{\partial t}+V_{ld}\frac{\partial V_{ld}}{\partial z}\right]+A\alpha_{ld}\frac{\partial P}{\partial z}+Ap_{ildv}\frac{\partial\alpha_{ld}}{\partial z}\\&=-A\Gamma_{ldv}(W_{idv}-V_{ld})+A\Gamma_e(V_{lc}-V_{ld})+A\tau_{idv}\\&+A\alpha_{ld}\rho_{ld}g_z\end{aligned} \tag{6}$$

The energy balance equations for the three phases can be written as:

Gas phase

$$A\frac{\partial}{\partial t}\left(\alpha_v\rho_v\left[H_v+\frac{V_v^2}{2}\right]\right)+\frac{\partial}{\partial z}\left(A\alpha_v\rho_v V_v\left[H_v+\frac{V_v^2}{2}\right]\right)-A\alpha_v\frac{\partial P}{\partial t}=A(q_{vic}+q_{vid})+\chi_c q_{wv}+A\Gamma_{lcv}\left[H_v+\frac{W_{icv}^2}{2}\right]+A\Gamma_{ldv}\left[H_v+\frac{W_{idv}^2}{2}\right]+A\alpha_v\rho_v V_v g_z \quad (7)$$

Continuous liquid field

$$A\frac{\partial}{\partial t}\left(\alpha_{lc}\rho_{lc}\left[H_{lc}+\frac{V_{lc}^2}{2}\right]\right)+\frac{\partial}{\partial z}\left(A\alpha_{lc}\rho_{lc}V_{lc}\left[H_{lc}+\frac{V_{lc}^2}{2}\right]\right)-A\alpha_{lc}\frac{\partial P}{\partial t}=Aq_{lci}+\chi_c q_{wlc}-A\Gamma_{lcv}\left[H_{lc}+\frac{W_{icv}^2}{2}\right]+A\Gamma_d\left[H_{ld}+\frac{V_{ld}^2}{2}\right]-A\Gamma_e\left[H_{lc}+\frac{V_{lc}^2}{2}\right]+A\alpha_{lc}\rho_{lc}V_{lc}g_z \quad (8)$$

Dispersed liquid field

$$A\frac{\partial}{\partial t}\left(\alpha_{ld}\rho_{ld}\left[H_{ld}+\frac{V_{ld}^2}{2}\right]\right)+\frac{\partial}{\partial z}\left(A\alpha_{ld}\rho_{ld}V_{ld}\left[H_{ld}+\frac{V_{ld}^2}{2}\right]\right)-A\alpha_{ld}\frac{\partial P}{\partial t}=Aq_{ldi}+\chi_c q_{wld}-A\Gamma_{ldv}\left[H_{ld}+\frac{W_{idv}^2}{2}\right]-A\Gamma_d\left[H_{ld}+\frac{V_{ld}^2}{2}\right]+A\Gamma_e\left[H_{lc}+\frac{V_{lc}^2}{2}\right]+A\alpha_{ld}\rho_{ld}V_{ld}g_z \quad (9)$$

Mass transfer terms Γ_{lcv} and Γ_{ldv} represent boiling/condensation and are positive for boiling and negative for condensation. Mass transfer terms Γ_e and Γ_d represent liquid droplet entrainment and deposition to (or from) the continuous liquid. Heat fluxes containing i in the subscript are fluxes between a field and its interface in front of another field (for example q_{ldi} means flux between liquid droplet and interface with vapour), while fluxes with a subscript w means wall to field (q_{wlc} means heat flux between wall and continuous liquid).

The terms containing the parameter R in Eqs. (4) and (5) account for stratification effects in horizontal flow; in the present case of vertical annular flow, R is set to zero.

The above set of nine conservation equations differs from the set of seven equations used by Hoyer [6] but is essentially the same to that used by Sugawara [9]. The constitutive laws for the various terms in the equations are, however, different, as will be seen below. The present formulation allows for the solution of the velocities directly while that of Sugawara solves for momentum as the solution variable.

3. Closure relations

A number of closure relations are required to evaluate many of the right hand side terms in the above set of equations. These represent interphase exchange, wall-phase exchange etc. These are usually flow regime-specific and those of specific interest to the present study are discussed here. For the full set of closure relations, the reader is referred to Valette and Jayanti [8].

3.1. Closure relations in the mass balance equations

The mass transfer terms appearing in the right hand side of the mass balance equations contain terms dealing with phase change (Γ_{lcv} and Γ_{ldv}) and those related to the hydrodynamic processes of entrainment and redeposition, Γ_e and Γ_d, respectively. The first two are obtained from heat balance at the liquid–steam interface. The mass transfer per unit volume due to phase change between the phases is given by

Mass transfer between continuous liquid and gas: Γ_{lcv}

$$\Gamma_{lcv}=\frac{q_{wic}\chi_c/A-q_{lci}-q_{vic}}{H_v-H_{lc}} \quad (10)$$

Mass transfer between dispersed liquid and gas: Γ_{ldv}

$$\Gamma_{ldv}=\frac{q_{wid}\chi_c/A-q_{ldi}-q_{vid}}{H_v-H_{ld}} \quad (11)$$

The evaluation of the various heat fluxes appearing in Eqs. (10) and (11) is discussed in Section 3.3 below.

The droplet entrainment flux, Γ_e, appearing in Eqs. (1) and (2) is modelled as a sum of the contributions from two processes, namely, entrainment arising from the shearing action of gas flowing over a wavy surface, Γ_{eh}, and creation of droplets in the process of nucleate boiling due to break-up of bubbles, Γ_{eb}. The first of these, Γ_{eh}, is evaluated using the empirical correlation of Hewitt and Govan [4]:

$$\Gamma_{eh}=5.75\times10^{-5}\frac{4}{D_h}\rho_v V_v\left[(\alpha_{lc}\rho_{lc}V_{lc}-\dot{m}_{lfc})^2\frac{D_h\rho_l}{\sigma\rho_v^2}\right]^{0.316} \quad \text{when } \alpha_{lc}\rho_{lc}V_{lc}\geqslant\dot{m}_{lfc} \quad (12)$$

and $\Gamma_{eh}=0$ when $\alpha_{lc}\rho_{lc}V_{lc}\leqslant\dot{m}_{lfc}$. Here, $\dot{m}_{lfc}$ is the minimum film flow rate necessary for entrainment and is given by

$$\dot{m}_{lfc}=\frac{\mu_l}{D_h}\exp\left(5.8504+0.4249\frac{\mu_v}{\mu_l}\sqrt{\frac{\rho_l}{\rho_v}}\right). \quad (13)$$

For the second source of entrainment associated with boiling, Γ_{eb}, Hoyer [6] used a dimensional correlation developed by Milashenko et al. [23] applicable in the pressure range of 50–100 bar for a specific tube diameter. In the present study, this term is modelled using the

dimensionless correlation proposed by Ueda et al. [24] using data from water, R-11 and R-113 systems:

$$\Gamma_{eb} = 4.77 \times 10^2 \Gamma_{lcv}^{2.5} \left[\frac{\alpha_{lc} D_h}{4\sigma\rho_v} \right]^{0.75} \quad \text{when } \Gamma_{lcv} \geqslant 0 \tag{14}$$

and $\Gamma_{eb} = 0$ when $\Gamma_{lcv} \leqslant 0$.

The droplet deposition flux, Γ_d, is evaluated based on the turbulent diffusion model of Hewitt and Govan [4]. An additional term, based on Hoyer [6], is used to account for the inhibition of droplet deposition by the steam flux caused by evaporation. Thus, the net deposition flux per unit volume, Γ_d, is evaluated as

$$\Gamma_d = \frac{4}{D_h} \rho_{ld} \frac{\alpha_{ld}}{\alpha_{ld} + \alpha_v} \max(k_d - k_q, 0) \tag{15}$$

where

$$k_d = 0.18153 \left(\frac{\rho_v D_h}{\sigma} \right)^{-1/2} \quad \text{if } \frac{\alpha_{ld}\rho_{ld}}{(\alpha_{ld} + \alpha_v)\rho_v} \leqslant 0.3$$

$$k_d = 0.083 \left(\frac{\rho_v D_h}{\sigma} \right)^{-1/2} \left(\frac{\alpha_{ld}\rho_{ld}}{(\alpha_{ld} + \alpha_v)} \right)^{-0.65} \quad \text{if } \frac{\alpha_{ld}\rho_{ld}}{(\alpha_{ld} + \alpha_v)\rho_v} \geqslant 0.3$$

$$k_q = \frac{\Gamma_{lcv}}{0.065\rho_{lc}} \frac{D_h}{4} \frac{1}{\sqrt{\alpha_{ld} + \alpha_v}}$$

3.2. Closure relations for terms in the momentum balance equations

Closure relations are required to deal with momentum exchange due to the wall-phase interaction and due to inter-phase interaction. Of the latter, momentum exchange terms associated with mass transfer are already included in the momentum balance equations and do not require further modelling. In the present model, any momentum exchange resulting from friction between the wall and the dispersed phase due to bouncing etc. is neglected and hence the corresponding term is set to zero. For the other two phases, the coefficient C_k appearing in the respective momentum equations is evaluated as

$$C_k = \text{Max}\left\{ \frac{16}{Re_k}, \frac{0.079}{Re_k^{0.25}}, 0.005 \right\} \quad \text{with} \quad Re_k = \frac{\alpha_k \rho_k |V_k| D_h}{\mu_k} \tag{16}$$

If the wall is wetted by a liquid film, then the wall–gas momentum exchange is zero. It is found that wall–liquid film interaction does not contribute much to the pressure gradient in annular flow and it has even smaller influence on the dryout and post-dryout heat transfer. Hence the above simple modelling is thought to be sufficient.

The friction-related interfacial momentum exchange involves three terms: the liquid droplet–liquid film exchange, the liquid film–gas exchange and the liquid droplet–gas exchange. The first one is neglected while the last one is dealt with using a classical formulation of droplet drag in a gas flow with a constant drag coefficient, C_d, of 0.5. For vanishingly small liquid droplet volume fraction, a multiplicative function, $k_1(\alpha_{ld})$, is used to make the interfacial drag very large so that the droplets move with the velocity of the gas. Thus, the gas–droplet interfacial shear stress is given by

$$\tau_{idv} = \frac{1}{2} \frac{6\alpha_{ld}}{\delta} C_d \rho_v |V_v - V_{ld}| (V_v - V_{ld}) k_1(\alpha_{ld}) \tag{17}$$

where δ is the droplet diameter.

The interfacial friction between the continuous liquid phase and the gas phase is strongly flow regime-dependent. For annular flow conditions, a number of correlations exist to calculate the interfacial friction factor. Most of these are obtained from air–water data at near-atmospheric pressures. Extension of these, for example, that of Asali et al. [25], to typical high pressure annular flow conditions is found to result in over-prediction of the order of 100%. The use of the simple correlation of Wallis [26] is found to overpredict the adiabatic annular flow data of Wurtz [17] by about 35%. Keeping in mind that the phasic Reynolds numbers and the liquid film phase fraction under typical high pressure conditions can be very different from those for low pressure air–water systems, a purely geometric relation, based on the single-phase flow through fully-rough pipes (thus there being no influence of gas phase Reynolds number on the friction factor) is used to evaluate the interfacial friction factor:

$$f_i = \frac{0.331}{\left[\ln\left(\frac{k_s}{3.71 D_h} \right) \right]^2} \tag{18a}$$

where

$$\frac{k_s}{D_h} = 2.25 \alpha_{lc}^{1.7} \tag{18b}$$

It should be noted that Eq. (18a) does not introduce any new constants as it can be derived from the Colebrook–White formula for single-phase flow through fully-rough pipes. Eq. (18b) for the equivalent sand grain roughness of a flowing liquid film however is an empirical fit obtained to give good prediction of the pressure gradient for the data of Wurtz [17] as discussed below. The interfacial shear stress between the gas and the liquid film is evaluated as

$$\tau_{icv} = \frac{4}{D_h} \left(1 - \frac{\alpha_{lc}}{2} \right) f_i \rho_v |V_v - V_{lc}| (V_v - V_{lc}) \tag{19}$$

It remains to specify the interfacial velocities between the gas and the liquid phases. The interface between the gas and the liquid droplets is supposed to be moving at velocity of the droplet. Hence, W_{idv} is set to be equal to V_{ld}. In the case of the interface between the gas and the continuous liquid, the relation for the two-fluid model used in CATHARE [22] is adapted as:

$$W_{icv} = \frac{\alpha_v}{\alpha_v + \alpha_{lc}} V_{lc} + \frac{\alpha_{lc}}{\alpha_v + \alpha_{lc}} V_v \tag{20}$$

3.3. Closure relations for terms in the energy balance equations

It is necessary to specify the calculation scheme for the various heat fluxes appearing in the energy balance equations. These can be grouped under two categories: heat transfer involving the wall and interfacial heat transfers. It is assumed that the liquid droplets are not directly heated or cooled by the wall. Thus, q_{wld} and q_{wid} are set to zero. The heat transfer between the wall and the continuous liquid or the gas phase is modelled as being due to forced convection:

$$q_{wk} = \frac{\lambda_k}{D_h} Nu_{k,conv}(T_w - T_k) \tag{21}$$

where k refers to g or lc and the Nusselt number is obtained from the Dittus–Boelter equation. The flow is assumed to be turbulent, and the formulation obtained in tube geometry is applied also in more complex geometries such as rod bundles, using hydraulic diameter as a characteristic length instead of tube diameter:

$$Nu_{k,conv} = 0.023 Re_k^{0.8} Pr_k^{0.4} \quad \text{where } Re_k = \frac{|V_k| D_h}{\nu_k}$$

Following the practice in CATHARE [22], two cases are distinguished for the heat transfer between wall and continuous liquid interface, q_{wic}. When $T_w \geqslant T_{sat}(P)$, a nucleate boiling mode is assumed and the Thom correlation [2] is used to calculate the heat flux. When $T_w \leqslant T_{lc} \leqslant T_{sat}(P)$, heat transfer is assumed to occur by film condensation. A rough value of 2000 $W\,m^{-2}\,K^{-1}$ for film condensation heat transfer coefficient is used to calculate the heat flux. In all the other cases, q_{wic} is set to zero. Details can be found in Valette and Jayanti [8].

The heat flux between the gas and the interface of the dispersed liquid is evaluated using a convection law for flow around spheres [27]:

$$q_{vid} = \frac{6\alpha_{ld}}{\delta} Nu_{conv} \frac{\lambda_v}{\delta} (T_{sat} - T_v) \tag{22}$$

where

$$Nu_{conv} = 2 + 0.6 Re_v^{0.5} Pr_v^{1/3} \quad Re_v = \frac{\rho_v |V_v - V_{ld}| \delta}{\mu_v}$$

The heat flux between gas and the interface of continuous liquid is modelled using the forced convection approach:

$$q_{vic} = q_{vic,evap} = \frac{1}{\pi D_h} \frac{\lambda_v Nu_{evap}}{D_h} (T_{sat}(P_v) - T_v) \tag{23}$$

where

$$Nu_{evap} = 0.023 Re_v^{0.8} Pr_v^{0.4} \quad \text{with} \quad Re_v = \frac{\rho_v |V_v| D_h}{\mu_v}.$$

Finally, the heat flux between the dispersed liquid and its interface (q_{ldi}) and that between the continuous liquid and its interface (q_{lci}) are evaluated using a flashing or condensation formulation depending on whether the phasic temperature T_k is greater or less than saturation temperatures. This formulation allows the liquid phase temperatures to be close to the saturated conditions while allowing deviation from it, if necessary. This is not very relevant to the present study and full details can be found in Valette and Jayanti [8].

3.4. Other closure laws

Apart from the above relations, it is necessary to specify other empirical laws to completely determine the nature of the flow. These are discussed here.

The first of these concerns the transition to annular flow regime. Although annular flow has been studied and modelled extensively, it is one of least well-defined in terms of transition to annular flow. Often, purely empirical criteria are adopted to describe it in numerical calculations. Hewitt and Govan [4] used a quality of 0.01 to start their annular flow calculations. Sugawara [5] used a dimensional fit to the Baker's flow pattern map [28] to determine the transition. Hoyer [6] used a generalized minimum slip or maximum void fraction criterion to determine the transition between separated flows and dispersed flows. In terms of mechanistic modelling, there are generally two schools of thought [2] regarding this transition in vertical flow: that the superficial gas velocity should be higher than that required for flow reversal, expressed as

$$U_v^* = V_v \left(\frac{\rho_v}{(\rho_{lc} - \rho_v) g D_h} \right)^{0.5} > 1 \tag{24}$$

or that it should be high enough to suspend entrained droplets, which is often expressed as a Kutateladze number limitation

$$Ku_v = \alpha_v V_v \left(\frac{\rho_v^2}{[g\sigma(\rho_l - \rho_v)]} \right)^{\frac{1}{4}} > 3.2 \tag{25}$$

Both these criteria give nearly the same transition gas velocities at low pressures for typical tube diameters

used in dryout experiments. It is found that at high pressures, they predict very low transitional velocities to such an extent that implementation of these criteria would have resulted in annular flow at gas phase volumetric fraction of 0.1! On the other hand, imposition of a minimum "reasonable" gas phase volumetric fraction of 0.7 would delay the transition to annular flow so much that dryout could never be predicted accurately. This situation is illustrated in Fig. 4. In Fig. 4a, the predicted variation of gas fraction with quality is plotted at different pressures in the range of 30–200 bar for steam–water system while in Fig. 4b, the predicted quality at which a gas volume fraction of 0.7 is reached is plotted as a function of system pressure for typical flow conditions used in Becker et al. [18]. (These predictions are obtained from the models described above and are found to be relatively sensitive to the closure relations.) At low pressures, α_v of 0.7 is reached at qualities of less than 0.1; however, at a higher pressure of 100 bar, this limit is reached at a quality of 0.25; and at 200 bar, the quality has to be 0.5 before the void fraction reaches 0.7. If the annular flow transition is pegged at a minimum gas fraction of 0.7, dryout can occur only after a quality of 0.5 at a pressure of 200 bar. However, the dryout quality is significantly less, of order of 0.2–0.3, in many of Becker et al.'s experiments. The corresponding gas fraction, at dryout, would be in the range of 0.4–0.5. This brings into question the traditional conception, based on low pressure experiments, of annular flow as a high voidage core surrounded by a thin film of liquid.

Coming back to the question of annular flow transition, a mechanistic criterion is desirable. It is found that a constraint based only on U_v^* or Ku_v would be not sufficient as it may result in different void fractions at different mass flow rates. Given the relative insensitivity of the gas fraction vs quality curve to the mass flux, the following criterion is used to determine the onset of annular flow:

$$Ku_v > 3.2 \quad \text{and} \quad x > 0.1 \tag{26}$$

The limit of $x > 0.1$ may delay the onset of annular flow at low pressures; however, this would not affect the predictions of dryout and post-dryout heat transfer as dryout rarely occurs at such low qualities at low pressures. It is noted that the constant quality limit for the transition is in good agreement with the experimental results of Bergles et al. [29] for steam–water flow at a pressure of 69 bar. Reasonable agreement for high pressure dryout data in the range of 30 to 200 bar has been obtained with this criterion, as shown later.

The initial entrainment fraction is said to be a parameter of the calculation and Hewitt and Govan [4] showed that their results were sensitive to this parameter at high mass fluxes. In order to be consistent with the all-regime capability of the present model, the droplet volume fraction is set to a minimum value of 10^{-6} in all pre-annular flow cases where droplet field may not be present. Thus, the entrained fraction of liquid at the onset of annular flow is close to zero in all the cases considered here. Some test calculations for adiabatic flows have shown that the outlet conditions are not sensitive to the inlet entrainment fraction as the hydrodynamic equilibrium between entrainment and redeposition is reached fairly quickly. This may be an important parameter, especially at low liquid flow rates, if the flow at the inlet is two-phase and the zone of interest is close to the inlet.

The droplet diameter is an important parameter in determining, for example, the post-dryout heat transfer. Possible factors which influence the droplet size in annular flow have been reviewed recently by Azzopardi [11]. Several correlations, in the form of a critical Weber number criterion, exist in the literature; however these

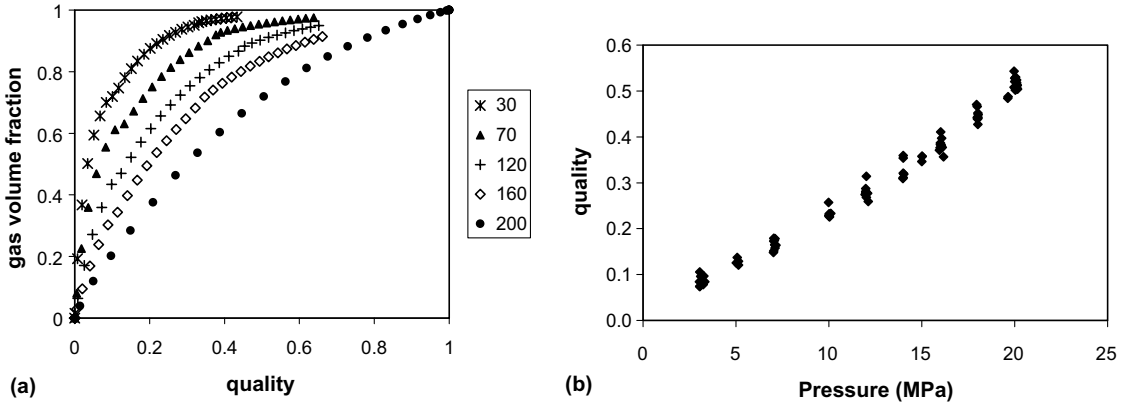

Fig. 4. (a) Calculated variation of gas volume fraction with quality at various pressures at a mass flux of 2000 $kg\,m^{-2}\,s^{-1}$, and (b) quality at which the gas volume fraction reaches 0.70 plotted as a function of pressure for the flow conditions of Becker et al. [18].

have been based principally on low pressure data of mostly air–water flows. Extension of these to typical high pressure dryout conditions results in drop sizes of the order 300–1000 μm, which is far above the typical size range of 30–200 μm in annular flow [11]. There appears, also, to be a droplet mass flux dependence on the drop size due to coalescence and Azzopardi [30] proposed a correlation for the Sauter mean diameter to take into account the droplet flux. This correlation, which is based on low pressure and low mass flux data, is found to give too large a size of droplets for some of the high mass flux cases of Bennett et al. [31]. In view of this, it is modified and approximated as follows to give better prediction of post-dryout heat transfer for the full range of mass fluxes in the experiments of Bennett et al. [31]:

$$\frac{\delta}{\ell} = (2.5We^{-0.58} + 0.1\alpha_{ld}^{0.25}) \tag{27}$$

Here ℓ is the Laplace length and the Weber number is defined based on the Laplace length:

$$\ell = \sqrt{\frac{\sigma}{g(\rho_{ld} - \rho_v)}} \quad We = \rho_v V_v^2 \ell/\sigma$$

It is found that the above correlation gave typical drop sizes of about 50 μm which is reasonable. The effect of this on the post-dryout heat transfer is illustrated in Fig. 5 for a specific case (Case no. 5335) of the data of Bennett et al. [31]. Here, the measured inside wall temperature data are compared with predictions using a drop size evaluation based on a critical Weber number criterion and as evaluated by Eq. (27). All the other aspects of the calculation are the same. It can be seen that greatly improved prediction is obtained by Eq. (27) while the prediction based on a critical Weber number predicts too high wall temperatures in the post-dryout region.

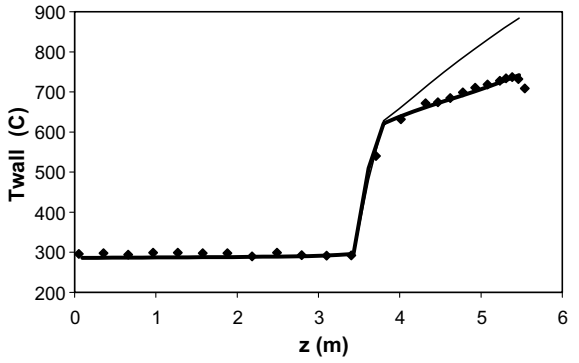

Fig. 5. Comparison with the data of Bennett et al. [31] for the case number 5335 of the predicted variation of the inside wall temperature using a droplet size correlation given by Eq. (27) (thick line) and that given by a critical Weber number of eight (thin line).

4. Numerical details

The above modelling has been used to predict adiabatic and diabatic flows with and without dryout in the pressure range of 30–200 bar. A brief description of the numerical solution procedure is in order before the results are presented. The set of conservation equations and closure relations is discretized using a finite difference scheme with staggered spatial mesh and the donor-cell method. A fully implicit scheme is used to deal with the temporal derivatives in which the terms dealing with interphase exchange, pressure propagation and convection are evaluated implicitly. This removes any Courant number limitation on the time step. The solution of the non-linear equations is carried out using the Newton–Raphson iterative method in which the Jacobian is re-evaluated at each iteration. Analytical derivatives for each equation and each closure relation are used systematically to evaluate the Jacobian. While there is no Courant number limitation on the time step, the non-linearity of the equations may cause convergence difficulties in case of large transients or at points of discontinuity in the constitutive models. An automatic scheme for the time step management is used to adjust the time step dynamically. Further details of the numerical algorithm are given by Barré et al. [32].

The calculations are carried out in a transient mode. Typically, the initial condition corresponds to subcooled liquid flowing through the tube at the given pressure and flow rate. Over a period of 10 s, the heat flux is linearly increased from zero to the final steady state value imposed in the experiments and all the boundary conditions are kept constant from that point onwards. The flow conditions and wall temperatures reach steady values, typically, in several seconds. Exploratory calculations were made for 30, 50 and 100 s to ensure that a steady state was reached and all subsequent calculations were carried out for 50 s. Typically, one calculation with 30 nodes took 1–2 min on a single CPU of the HP 9000/800 computer.

5. Results

The set of equations presented in Sections 2 and 3 constitutes the overall model used for the prediction of dryout and post-dryout heat transfer. The conservation equations are well-known and many of the closure relations have already been well-established for low pressure systems. Three parameters have been principally altered in the present study to make the model applicable to high pressure systems. These are (i) the equivalent sand grain roughness relation given in Eq. (18b); (ii) the additional constraint of quality for annular flow transition as in Eq. (26); and (iii) the modified drop size correlation given by Eq. (27). Some of the data cited

Table 1
Range of data used in the present study for predictions

Source	Range of pressure (bar)	Range of mass flux ($kg\,m^{-2}\,s^{-1}$)	Tube inner diameter (mm)	Parameters compared	Number of points used
Wurtz [17]	30–90	500–3000	10, 20	Pressure gradient, entrained fraction	74
Wurtz [17]	30–90	500–3000	10	Dryout quality	32
Bennett et al. [31]	70	350–5100	12.6	Dryout quality, post-dryout wall temperature	31
Becker et al. [18]	30–200	500–3000	10, 14.9, 24.7	Dryout quality, post-dryout wall temperature	88

below have been used to determine these relations and hence the results shown below cannot be treated as independent validation. The purpose however is to demonstrate that, with the above modelling, satisfactory predictions can be obtained over a wide range of systems pressures, mass flow rates and tube diameters.

The data set used for model validation is summarized in Table 1. It consists of adiabatic and diabatic results of Wurtz [17] in the pressure range of 30–90 bar in tubes of two diameters; systematic and coherent data of Bennett et al. [31] for dryout and post-dryout heat transfer in a single tube at a nominal pressure of 70 bar; and a large amount of dryout and post-dryout data from Becker et al. [18] covering systematically a wide range of pressures and mass flow rates in three tubes. Not all the available data is used in the validation; however, the data (or runs) for calculations have been selected in such a way as to cover the entire range of flow rates, heat fluxes and pressures contained in each data set. The results from these calculations are discussed below.

5.1. Data of Wurtz (1978)

The adiabatic data of Wurtz [17] were obtained in tubes of 10 and 20 mm inner diameter. The tests in the 10 mm diameter tube covered the pressure range of 30–90 bar while those in the 20 mm tube were carried out only at 70 bar. In both cases, the mass fluxes varied from 500–3000 $kg\,m^{-2}\,s^{-1}$ with qualities up to 0.6. The comparison between the predicted and the measured total pressure gradient and entrained mass flux for about 70 runs are shown in Fig. 6a and b, respectively. It can be seen that the pressure gradient is predicted well. Wurtz [17] estimated that most of the pressure gradient in these cases was the frictional component and this was found to be the case in the present study. The entrained mass fluxes shown in Fig. 6b show a larger scatter, but except for a few cases, all are reasonably well-predicted. The present calculations confirm the observation of Hoyer [6] that the dryout prediction is not very sensitive to the interfacial friction; the predicted entrained mass flux is found to be relatively insensitive to the closure relation for interfacial friction. Since the data considered here are adiabatic data, these tests verify the hydrodynamic component of entrainment and redeposition. The contribution of nucleate boiling component to both these important processes is not reflected either in the experiments or in the calculations as in both a sufficiently long tube (>400 tube diameters) is available for hydrodynamic equilibrium to be achieved.

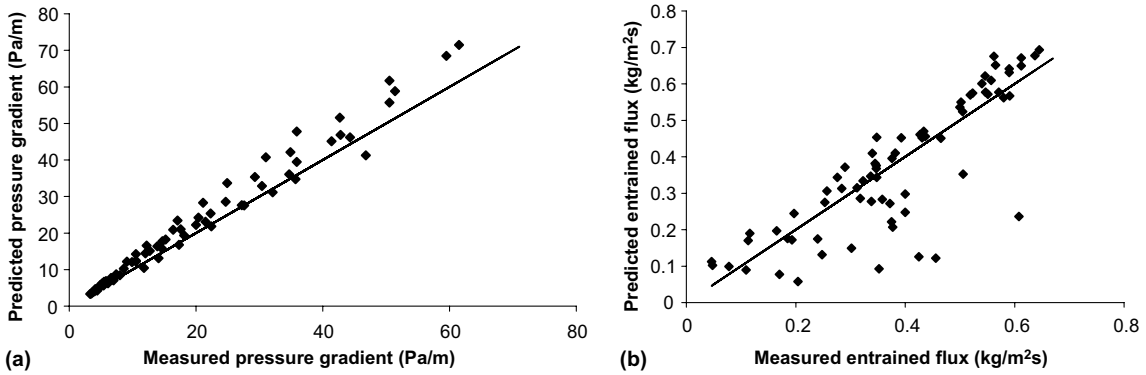

Fig. 6. Comparison with the adiabatic data of Wurtz [17] of (a) pressure gradient and (b) entrained droplet flux in the pressure range of 30–90 bar.

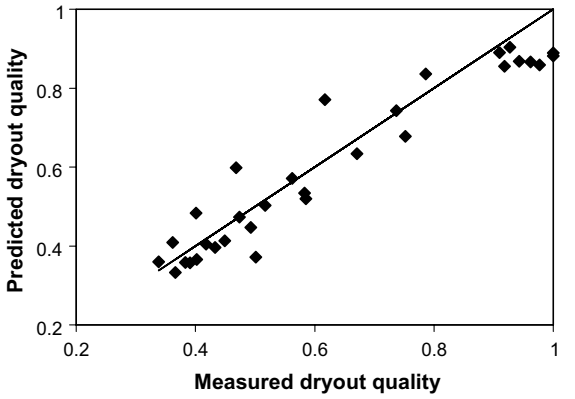

Fig. 7. Comparison of the predicted dryout quality with the experimental data of Wurtz [17] in the pressure range of 30–90 bar.

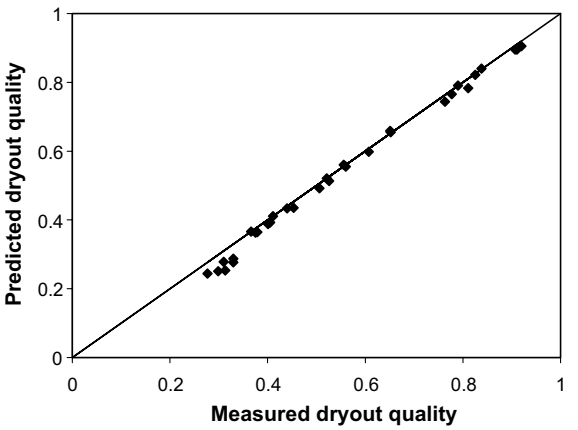

Fig. 8. Comparison of the predicted dryout quality with the experimental data of Bennett et al. [31] at an exit pressure of 70 bar.

The predictions of about 30 runs of the burnout experiments of Wurtz [17] in the 10 mm tube diameter are shown in Fig. 7. These cover the pressure range of 30–90 bar and the mass flux range of 500–3000 $\mathrm{kg\,m^{-2}\,s^{-1}}$. It can be seen that good agreement is once again obtained between the predictions and the experiments over the entire range of quality. No apparent pressure effect can be seen in the accuracy of the predictions.

5.2. Data of Bennett et al. (1967)

Bennett et al. [31] conducted systematic dryout and post-dryout experiments in a tube of 12.6 mm internal diameter using Inconel as material for the tube so as to avoid the temperature dependence of electrical resistivity exhibited by stainless steel. Although the experiments were conducted at a single pressure of 70 bar, the mass flux was varied in the wide range of 350–5000 $\mathrm{kg\,m^{-2}\,s^{-1}}$. The effect of heat flux was also studied systematically at each flow rate by taking wall temperature measurements at several increments of heat fluxes. The dryout data therefore reflect well the non-equilibrium effects associated with developing flow in a heated tube. Comparison of the predicted and the experimental dryout quality (Fig. 8) shows excellent agreement between the two. This shows that heat flux effects on the net entrainment flux are well-captured in the correlations and provide an indirect validation of these aspects of the correlations.

The post-dryout heat transfer predictions also show good agreement with the data and exhibit the correct trends. This is illustrated in Fig. 9 where the measured wall temperatures for mass fluxes of 350, 650, 1000, 2000, 3800 and 5100 are compared with the data. It can be seen that excellent agreement is there between the two for all the cases. The extent of temperature rise and the further evolution of the inside wall temperature and the variation of these with mass flux are captured quite well. It is noted here that a drop size correlation based on a critical Weber number of eight would have not captured all these effects accurately, the deviation in many cases being more like that shown in Fig. 5. These calculations serve therefore to especially validate the drop size correlation developed as part of the present study.

5.3. Data of Becker et al. (Ref. [18])

These data cover dryout and post-dryout heat transfer in the range of 30–200 bar of pressure and 500–3000 $\mathrm{kg\,m^{-2}\,s^{-1}}$ of mass flux in tubes of 10 and 14.9 mm internal diameter. Additional data from a tube of 24.7 mm internal diameter were reported in the pressure range of 150 and 200 bar and in the mass flux range of 800–2400 $\mathrm{kg\,m^{-2}\,s^{-1}}$. The outside wall temperature was measured in a stainless steel tube and the inside wall temperature was deduced from the known heat flux. The inlet subcooling was kept at 10 °C in most of the cases and at 5 °C in the rest of the cases. The comparison between the predicted and the measured dryout quality is shown in Fig. 10 where the data are sorted according to pressure (Fig. 10a), mass flux (Fig. 10b) and tube diameter (Fig. 10c). It can be seen that although there is a large scatter, the predictions are quite satisfactory given that the predictions go right up to a relative pressure, P/P_{cr}, of 0.9. Unlike in the case of Bennett et al. [31], the experimental data of Becker et al. [18] themselves exhibit considerable scatter in the sense that non-monotonic effect of heat flux on dryout quality is

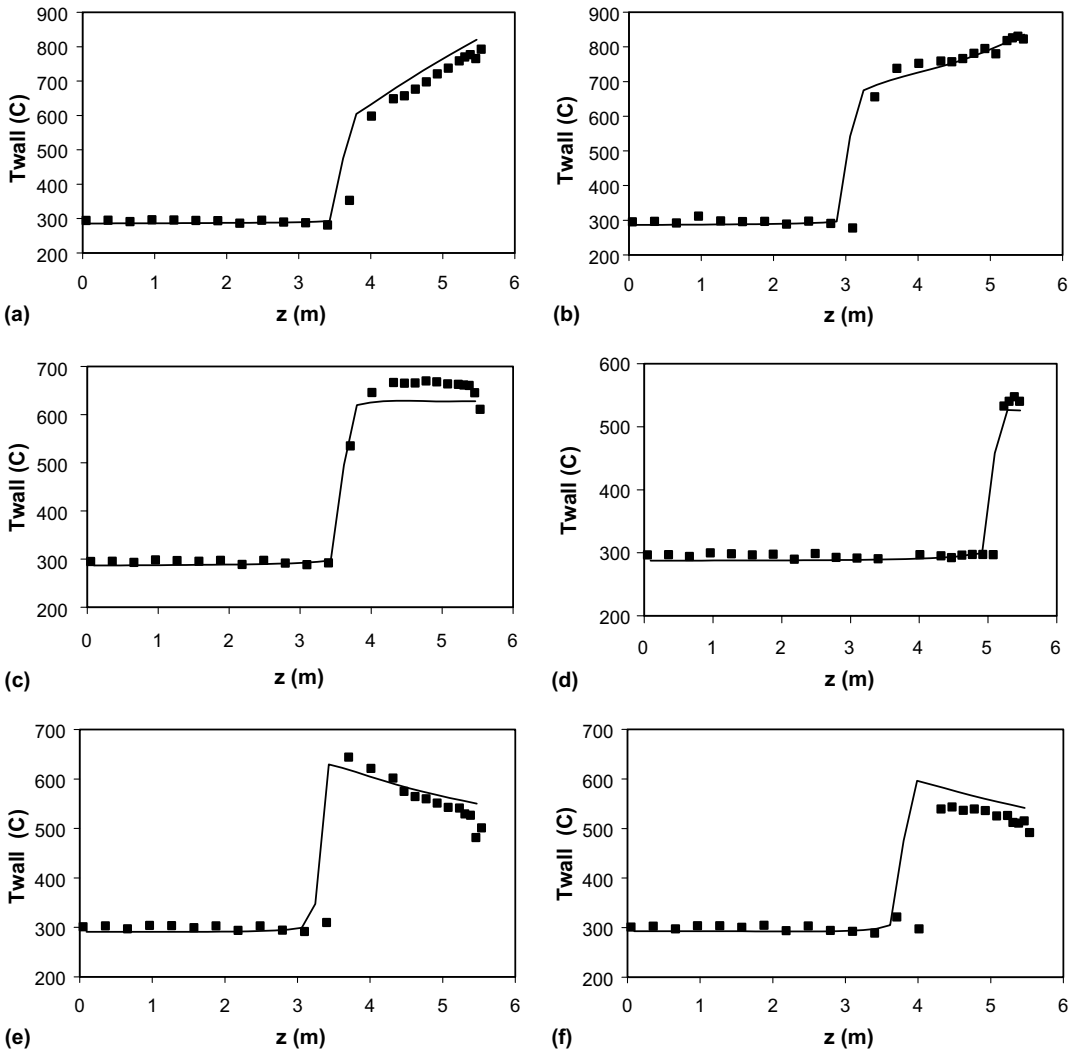

Fig. 9. Comparison of the predicted inside wall temperature with the data of Bennett et al. [31] at 70 bar for a mass flux of (a) 380, (b) 650, (c) 1020, (d) 1950, (e) 3800 and (f) 5180 $kg\,m^{-2}\,s^{-1}$. The corresponding heat fluxes are 512, 850, 921, 918, 1704 and 1837 $kW\,m^{-2}$.

observed in a number of cases. For example, an increase in heat flux in some cases would have no effect on the dryout quality, a large effect in some cases and a non-monotonic effect in some other cases. Close study of these trends showed these *not* to be a systematic effect of pressure. The categorized data shown in Fig. 10a–c show that the accuracy of prediction is rather insensitive to the tube diameter (in the range of 10 mm to 25 mm). There appears to be an overprediction of dryout quality for some cases of low mass flux (500 and 1000 $kg\,m^{-2}\,s^{-1}$), as indicated in Fig. 10b, in the pressure range of 100–160 bar. It has been found that the term representing boiling-induced entrainment (Eq. (14)) becomes significant under these conditions; better modelling of this term may improve the results. It is felt that a revision of the modelling of all the entrainment and redeposition processes would be more appropriate given the 300-fold change in the ratio of densities of the two phases between atmospheric pressure and 200 bar.

The predicted wall temperatures in the post-dryout heat transfer are shown in Fig. 11. Here, the wall temperatures for a constant mass flux of 1000 $kg\,m^{-2}\,s^{-1}$ and inlet subcooling of 10 K are shown at different pressures with the heat flux such that the dryout occurs nearly at the same location. Comparison with Fig. 3 shows that the effect of pressure, namely, significant reduction in the temperature jump immediately after dryout, is well-predicted. Specific comparison with se-

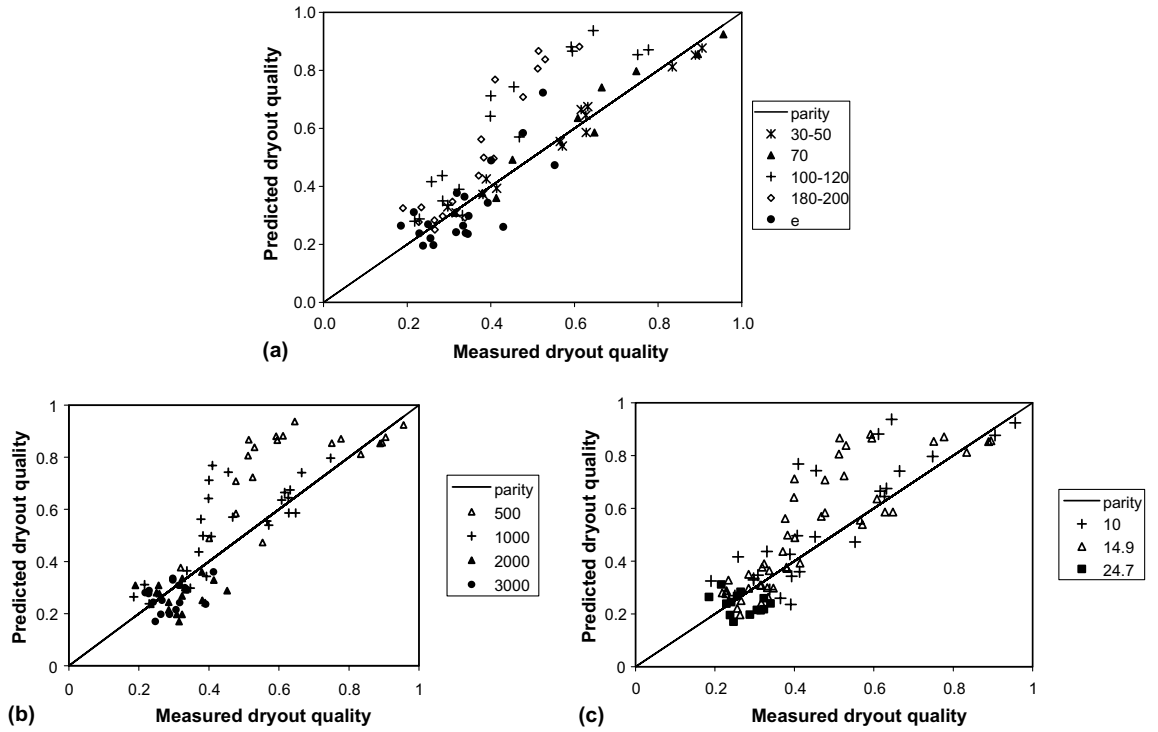

Fig. 10. Comparison of the predicted dryout quality with the experimental data of Becker et al. [18] with the data sorted according to (a) pressure, (b) mass flux and (c) tube diameter.

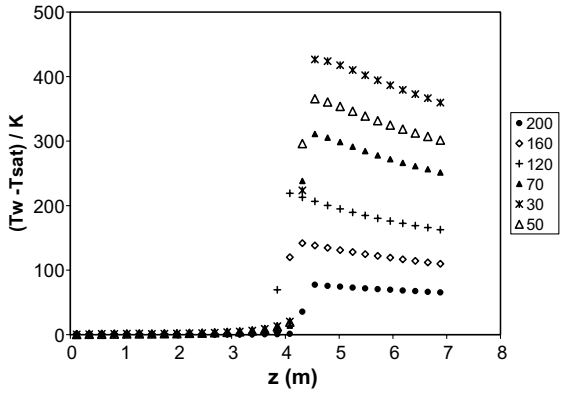

Fig. 11. Predicted variation of the inside wall temperature along the tube at different pressures for a mass flux of 2000 $kg\,m^{-2}\,s^{-1}$. The heat flux is adjusted such that dryout occurs at nearly the same location.

lected cases from Becker et al. [18] are shown in Figs. 12–14 at system pressures of 70, 160 and 200 bar, respectively, for mass fluxes of 500, 1000, 2000 and 3000 $kg\,m^{-2}\,s^{-1}$. Fairly good agreement (but not as good as for the data of Bennett et al., see Fig. 10) is obtained at 70 bar. At higher pressures, the trend with mass flux and pressure are predicted well but there is a significant overprediction of the wall temperature at high pressure, high mass flux conditions (e.g., Fig. 14a and b). This may be due to the complicated nature of the flow under these conditions wherein the droplet volume fraction may be in excess of 0.2! It is possible that droplet–wall interaction, which is neglected in the present study, has a significant impact on the heat transfer under these conditions. More study is clearly required to quantify these effects.

6. Conclusions

A comprehensive set of closure relations is presented in the context of a one-dimensional three-phase calculation methodology for the prediction of dryout and post-dryout heat transfer at high pressures. New correlations have been developed for the interfacial friction factor between the liquid film and the gas phase; for the droplet diameter and for the transition to annular flow.

Comparison with the data of Bennett et al. [31], Wurtz [17] and Becker et al. [18] shows that fairly accurate predictions of the dryout quality can be obtained in the pressure range of 30–200 bar, mass flux range of 500–5000 $kg/m^2\,s$ and tube diameter range of 10–25 mm.

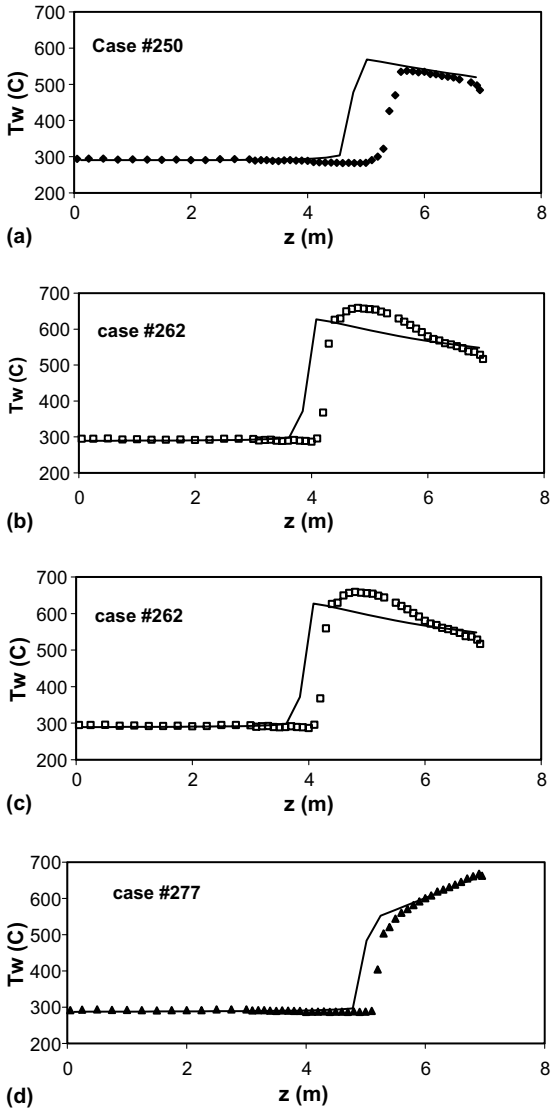

Fig. 12. Comparison of the predicted temperature variation with the data of Becker et al. [18] at a pressure of 70 bar at mass fluxes of (a) 3000, (b) 2000, (c), 1000 and (d) 500 $\mathrm{kg\,m^{-2}\,s^{-1}}$. The corresponding case numbers are given in the figure.

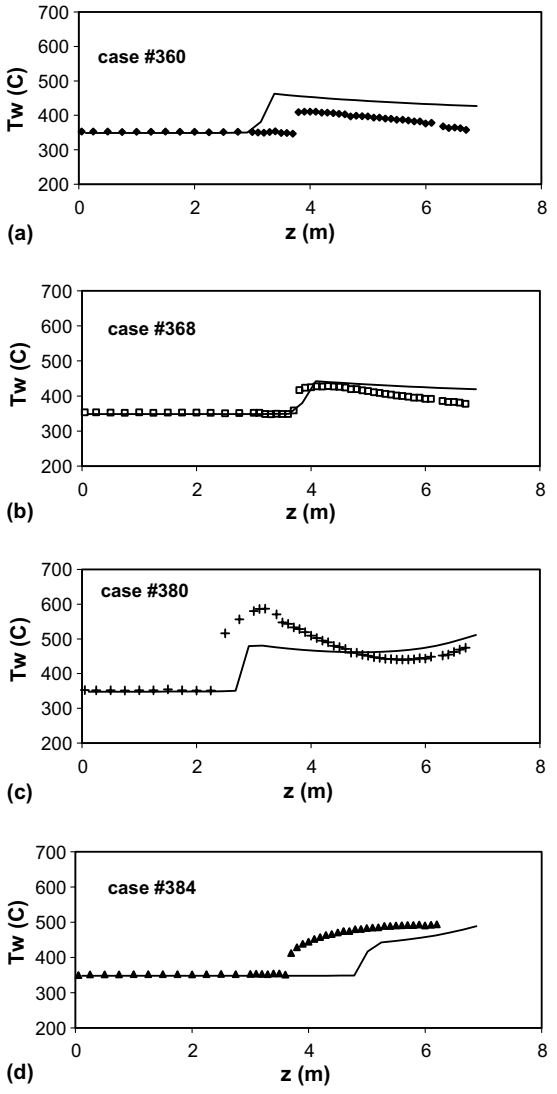

Fig. 13. Comparison of the predicted temperature variation with the data of Becker et al. [18] at a pressure of 160 bar at mass fluxes of (a) 3000, (b) 2000, (c), 1000 and (d) 500 $\mathrm{kg\,m^{-2}\,s^{-1}}$. The corresponding case numbers are given in the figure.

Good agreement for the post-dryout heat transfer is obtained with the data of Bennett et al. [31] at 70 bar over the entire range of mass fluxes. The wall temperature in the post-dryout condition is overpredicted under some conditions (combination of high pressure and high mass flux) of Becker et al. [18]. This may be due to neglect of wall–droplet field interaction.

The present calculations indicate that at high pressures, i.e., for relative pressure, $P/P_{cr} > 0.5$, annular flow-type conditions may prevail even for gas phase volume fractions <0.5 and the droplet phase volume fractions may be very high, of the order of 0.2 or higher. This is very different from the traditional picture of annular flow having a very thin liquid film ($\alpha_{lc} < 0.02$ in most air–water data) and a high-voidage ($\alpha_v > 0.9$) core. The mechanism of boiling-induced entrainment, rather than the traditional route of gas-shear induced hydrodynamic entrainment, appears to dominate the entrainment process under these conditions. Experimental verification of these trends would be very useful to further validate the present modelling.

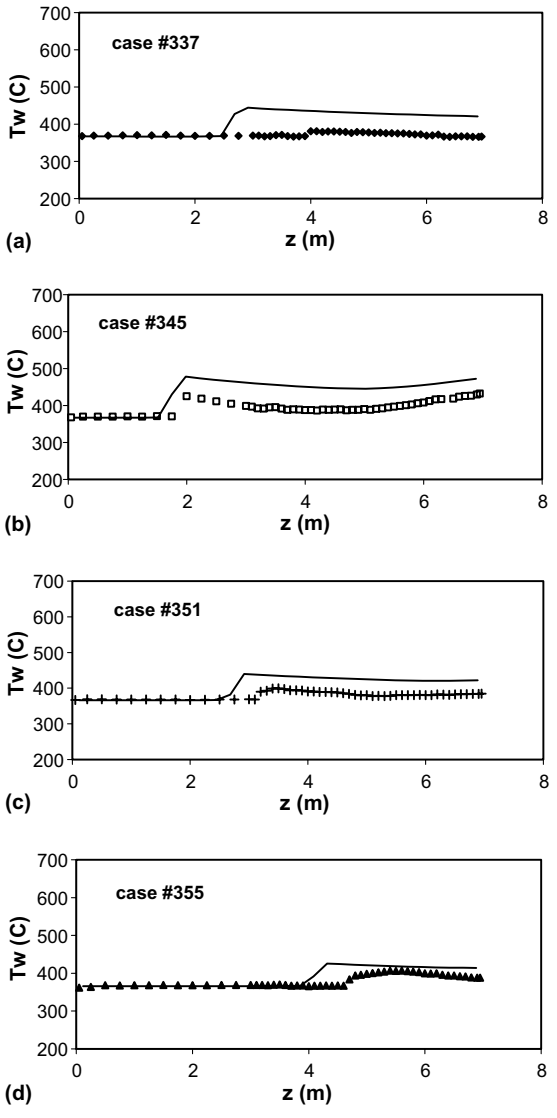

Fig. 14. Comparison of the predicted temperature variation with the data of Becker et al. [18] at a pressure of 200 bar at mass fluxes of (a) 3000, (b) 2000, (c), 1000 and (d) 500 $kg\,m^{-2}\,s^{-1}$. The corresponding case numbers are given in the figure.

Acknowledgements

This work was supported by the Commissariat à l'Energie Atomique (CEA, France), Electricité de France (EDF), the Institut de Radioprotection et de Sûreté Nucléaire (IRSN, France) and FRAMATOME-ANP.

References

[1] G.F. Hewitt, N.S. Hall-Taylor, Annular Two-phase Flow, Pergamon, Oxford, UK, 1970.

[2] J.G. Collier, Convective Boiling and Condensation, McGraw-Hill, New York, USA, 1981.

[3] P.B. Whalley, P. Hutchinson, G.F. Hewitt, The calculation of critical heat flux in forced convective boiling, in: Proceedings of 5th International Heat Transfer Conference, Tokyo, 1974, Paper no. B6.11.

[4] G.F. Hewitt, A.H. Govan, Phenomenological modelling of non-equilibrium flows with phase change, Int. J. Heat Mass Transfer 33 (1990) 229–242.

[5] S. Sugawara, Analytical prediction of CHF by FIDAS code based on three-fluid film-dryout model, J. Nucl. Sci. Technol. 27 (1990) 12–29.

[6] N. Hoyer, Calculation of dryout and post-dryout heat transfer for tube geometry, Int. J. Multiphase Flow 24 (1998) 319–334.

[7] C. Frepoli, L.E. Hochreiter, A.J. Ireland, K. Ivanov, Modelling of annular film dryout with COBRA-TF, in: Proceedings of the 9th International Conference On Nuclear Engineering, ICONE-9, Lyon, France, 2001.

[8] M. Valette, S. Jayanti, Annular dispersed flow calculations with a two-phase three-field model, in: Proceedings of European Two-Phase Flow Group Meeting, Norway 12–13 May, 2003.

[9] S. Sugawara, Droplet deposition and entrainment modelling based on three-fluid model, Nucl. Eng. Des. 122 (1990) 67–84.

[10] R.I. Nigmatulin, B.I. Nigmatulin, Y.D. Khodzhaev, V.E. Kroshilin, Entrainment and deposition rates in a dispersed film flow, Int. J. Multiphase Flow 22 (1996) 19–30.

[11] B.J. Azzopardi, Drops in annular two-phase flow, Int. J. Multiphase Flow 23 (Suppl.) (1997) 1–53.

[12] I. Kataoka, M. Ishii, A. Nakayama, Entrainment and deposition rates of droplets in annular two-phase flow, Int. J. Heat Mass Transfer 43 (2000) 1573–1589.

[13] T. Kitahara, T. Okawa, K. Yoshida, T. Matsumoto, I. Kataoka, Improved correlations for annular flow simulation in annuli based on a one-dimensional multi-fluid model, in: Proceedings of 4th International Conference Multiphase Flow, New Orleans, USA,, May 27–June 1 2001.

[14] L. Pan, T.J. Hanratty, Correlation of entrainment for annular flow in vertical pipes, Int. J. Multiphase Flow 28 (2002) 363–384.

[15] A.W. Bennett, G.F. Hewitt, H.A. Kearsey, R.F.K. Keeys, D.J. Pulling, Studies of burnout in boiling heat transfer to water in round tubes with non-uniform heating, UKAEA Report No. AERE - R 5076, 1966.

[16] R.F.K. Keeys, J.C. Ralph, D.N. Roberts, The effect of heat flux on liquid entrainment in steam–water flow in a vertical tube at 1000 psia, UKAEA Report No. AERE-R 6294, 1966.

[17] J. Wurtz, An experimental and theoretical investigation of annular steam–water flow in tubes and annuli at 30 to 90 bar, RISØ Report No. 372, April 1978.

[18] K.M. Becker, C.H. Ling, S. Hedberg, G. Strand, An experimental investigation of post dryout heat transfer, Department of Nuclear Reactor Engineering, Royal Institute of Technology report KTH-NEL-33, Stockholm, Sweden, 1983.

[19] K.M. Becker, P. Askeljung, S. Hedberg, B. Söderquist, U. Kahlbom, An experimental investigation of the influence of

axial heat flux distributions on post dryout heat transfer for flow of water in vertical tubes, Department of Nuclear Reactor Engineering, Royal Institute of Technology report KTH-NEL-54, Stockholm, Sweden, 1992.

[20] S.P. Antal, M.Z. Podowski, R.T. Lahey, A contribution to mechanistic multidimensional modelling of annular flows, in: Proceedings of the 34th National Heat Transfer Conference, Pittsburgh, Pa, Aug. 20–22 2000, Paper No. NHTC2000-12247.

[21] B.N. Kishore, S. Jayanti, A CFD-based model for annular gas–liquid flow, INSPEC-03, IIT-Bombay, Mumbai, India, January 2003.

[22] D. Bestion, The physical closure laws in the CATHARE code, Nucl. Eng. Des. 124 (1990) 229–245.

[23] V.I. Milashenko, B.I. Nigmatulin, V.V. Petukhov, N.I. Trubkin, Burnout and distribution of liquid in evaporative channels of various lengths, Int. J. Multiphase Flow 15 (1989) 393–402.

[24] T. Ueda, M. Inoue, S. Nagatome, Critical heat flux and droplet entrainment rate in boiling of falling liquid films, Int. J. Heat Mass Transfer 24 (1981) 1257–1266.

[25] J.C. Asali, T.J. Hanratty, P. Andreussi, Interfacial drag and film height for vertical annular flow, AIChE J. 31 (1985) 895–902.

[26] G.B. Wallis, One-dimensional two-phase flow, McGraw-Hill, New York, USA, 1969.

[27] R.B. Bird, W.E. Stewart, E.N. Lightfoot, Transport Phenomena, Wiley, New York, USA, 1969.

[28] O. Baker, Design of pipelines for simultaneous flow of oil and gas, Oil Gas J. (1954) 26.

[29] A.E. Bergles, J.P. Roos, J.G. Bourne, Investigation of boiling flow regimes and critical heat flux, NYO-3304-13, 1968.

[30] B.J. Azzopardi, Drop sizes in annular two-phase flow, Exp. Fluids 3 (1985) 53–59.

[31] A.W. Bennett, G.F. Hewitt, H.A. Kearsey, R.F.K. Keeys, Heat transfer to steam–water mixtures flowing in uniformly heated tubes in which the critical heat flux has been exceeded, UKAEA Report No. AERE - R 5373, 1967.

[32] F. Barré, M. Parent, B. Brun, Advanced numerical methods for thermalhydraulics, Nucl. Eng. Des. 145 (1993) 147–158.